Surveying the Protostellar Population Powering Extended Green Objects (EGOs) with the VLA

A. P. M. Towner[1*,2**], C. L. Brogan[2], T. R. Hunter[2]

[1]University of Virginia, [2]National Radio Astronomy Observatory

[*]at4bu@virginia.edu [**]A. P. M. Towner is supported by the Grote Reber Doctoral Fellowship program

Abstract

On sizescales of 0.1 pc, Extended Green Objects (EGOs, so named due to their extended 4.5 micron emission; Cyganowski et al. 2008) are thought to harbor massive young stellar objects in an evolutionary phase in which mass accretion is actively driving outflows. We have been conducting a multi-wavelength examination of a sample of EGOs in the Milky Way with distances of 1 to 5 kpc. Here, we present JVLA 1.3 cm (K-band) observations of 8 of these objects, all of which are now thought to be massive protoclusters. These protoclusters are typical young, massive objects with total FIR luminosities ranging from 1,000 to 40,000 L_{sun}, and exist in a specific evolutionary state that is a) prior to the onset of significant ionization feedback and b) in which active outflows dominate their infrared appearance.

The JVLA observations presented herein target 1.3 cm (K-band) continuum emission, with sensitivities of ~10 μJy at a typical angular resolution of 0.3". We utilize complementary ALMA 7m+12m Band 6 (1.3 mm) observations in order to calculate the spectral index of each 1.3 cm detection, and therefore determine whether free-free emission may be present. The observations also include known 22 GHz H_2O masers, which are associated with protostellar outflows and are thought to originate in fast shocks (Cyganowski et al. 2013, and references therein); therefore, the presence of H_2O masers allows us to explore some of the outflow activity in these sources as well as how it relates to the continuum emission. Our eventual goal for this project is to characterize the nature and onset of centimeter-wavelength continuum emission when it first appears in massive YSOs.

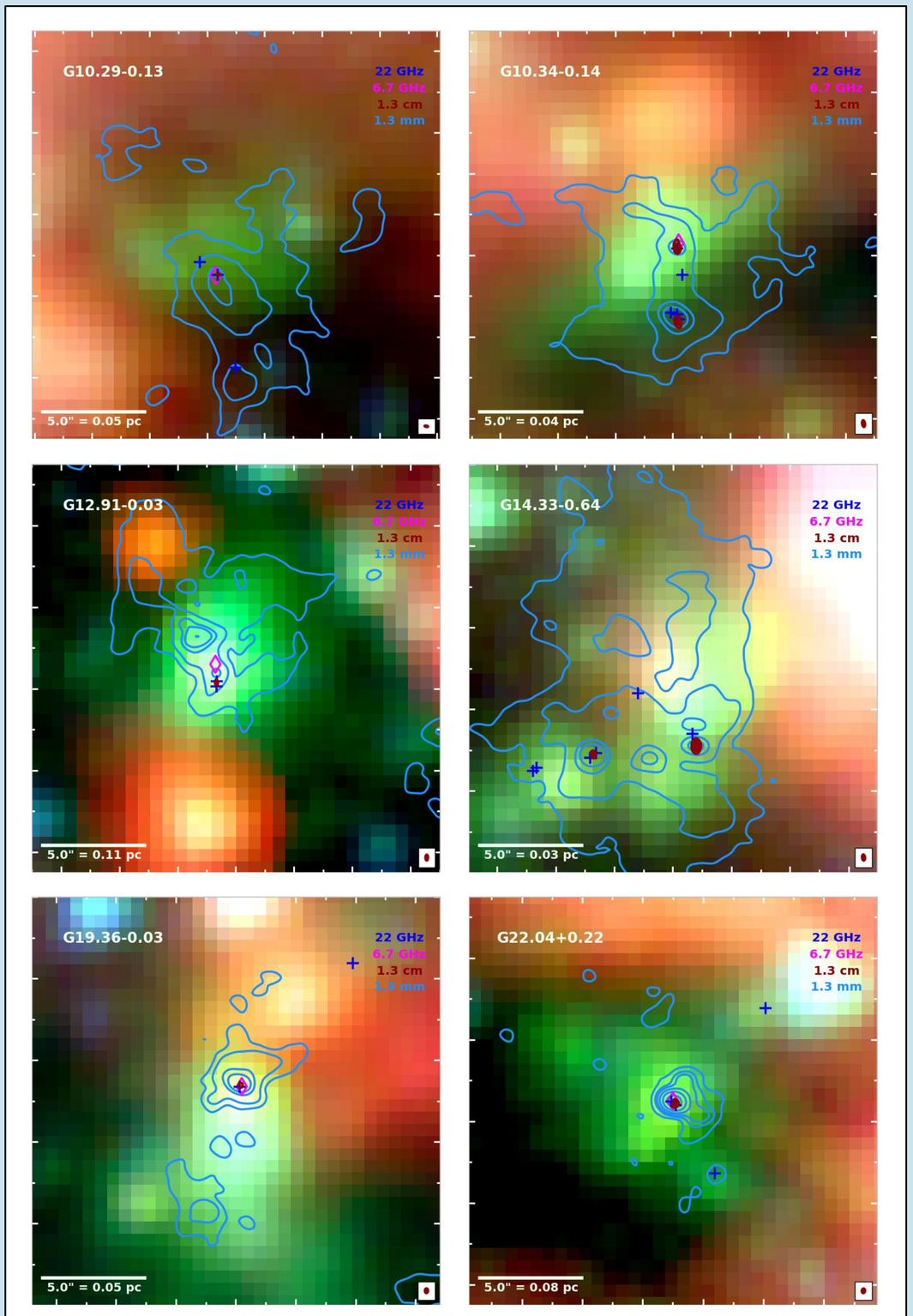

Figure 1. RGB images of four of our EGOs with 1.3 cm (dark red) and 1.3 mm (light blue) continuum contours overlaid. R, G, and B in the background images correspond to 8.0, 4.5, and 3.6 μm emission, respectively (*Spitzer* IRAC). 22 GHz water masers are marked with dark blue crosses, and 6.7 Class II methanol masers are marked with magenta diamonds. The JVLA K-band beam is shown in the lower right corner of each image. Contour levels are [5, 10] x rms for the 1.3 cm data, and [10,35,100,150,350,800] x rms for the 1.3 mm data.

Results and Analysis

We have imaged the 1.3 cm continuum and 22 GHz H_2O maser data for eight of the sources in our sample, and detected both 1.3 cm continuum and 22 GHz maser emission in all eight. In all cases, at least 3 individual maser spots are present, but most sources have 5 or more. In all but one case, at least one continuum source lies at the center of the EGO and has a clear 1.3 mm counterpart. We consider such detections to be likely EGO-associated. The one EGO for which there are no 1.3 cm detections toward the EGO center, G18.89-0.47, also does not have any clear 1.3 mm counterparts for the 1.3 cm emission.

For our likely EGO-associated 1.3 cm detections, the continuum emission is typically unresolved, and the few resolved sources are all smaller than 0.4 x 0.4 arcsec in size. Table 1 shows our preliminary results for each 1.3 cm detection: position, 1.3 cm and corresponding 1.3 mm flux densities, and spectral index (α). The spectral indices were calculated according to the equation: $\alpha = d\log(S_\nu) / d\log(\nu)$. In cases where there are multiple 1.3 cm detections, sources are listed according to their relative positions in the FOV (e.g. E for the eastern source, etc). The 1.3 cm and 1.3 mm flux densities have typical rms values of 12 μJy and 0.2 mJy respectively. 1.3 cm fluxes and positions were obtained by fitting 2D gaussians to the emission; 1.3 mm emission was fit with 2D gaussians where possible, but in some cases had to be estimated with a polygonal aperture due to source morphology (G28.83-0.25_W) or estimated as an upper limit due to the lack of any distinct 1.3 mm counterpart to the 1.3 cm emission (G18.89-0.47, both sources).

Assuming a dust contribution of $\beta = 1.7$, and taking $\alpha = \beta + 2$ in the case of only optically thin dust emission, we find that every EGO-associated 1.3 cm source in our sample has a spectral index too shallow (< 3.7) to be attributed to dust emission alone. Some processes with a negative spectral index (e.g. an HII region or synchrotron emission) must be contributing to α as well.

Figure 1 shows our 1.3 cm and 1.3 mm results for six representative sources in our sample; the radio-wavelength contours are overlaid on a 3-color image with IRAC 8.0, 4.5, and 3.6 μm data mapped to R, G, and B, respectively. Water masers (tracing outflow activity) are shown as blue crosses, and 6.7 GHz Class II CH_3OH (methanol) masers – which are associated exclusively with high-mass YSOs, as they are the only YSOs massive enough to produce the higher-energy radiation required to pump Class II masers – are indicated by magenta diamonds. The 6.7 GHz maser positions are from Cyganowski et al. (2009) for all sources shown except G1291-0.03, which is from Green et al. (2010).

TABLE 1
PROPERTIES OF EGO 1.3 CM DETECTIONS

Source	Coordinates (J2000) RA ($h\ m\ s$)	Dec (° ′ ″)	1.3 cm Flux Density (μJy)	1.3 mm Flux Density (mJy)	Spectral Index (α)
G10.29–0.13	18:08:49.3603 (0.0008)	-20:05:58.936 (0.003)	89 (13)	28 (2)	2.50
G10.34–0.14_N	18:08:59.9853 (0.0004)	-20:03:35.61 (0.02)	194 (18)	46 (5)	2.38
G10.34–0.14_S	18:08:59.9827 (0.0005)	-20:03:39.26 (0.02)	210 (50)	170 (14)	2.88
G12.91–0.03	18:13:48.2662 (0.0001)	-17:45:39.70 (0.01)	107 (8)	25 (1)	2.37
G14.33–0.64_E	18:18:54.6715 (0.0002)	-16:47:50.222 (0.005)	300 (13)	370 (38)	3.09
G14.33–0.64_W	18:18:54.3202 (0.0001)	-16:47:49.813 (0.002)	1710 (33)	142 (18)	1.92
G18.89–0.47_NE	18:27:08.4814 (0.0001)	-12:41:29.305 (0.004)	131 (6)	<0.96	<0.87[a]
G18.89–0.47_SW	18:27:08.2988 (0.0004)	-12:41:32.76 (0.01)	601 (5)	<0.23	<-0.42[a]
G19.36–0.03	18:26:25.7837 (0.0002)	-12:03:53.237 (0.004)	142 (8)	129 (11)	2.96
G22.04+0.22	18:30:34.6924 (0.0008)	-9:34:47.13 (0.02)	196 (33)	227 (13)	3.06
G28.83–0.25_E	18:44:51.0824 (0.0001)	-3:45:48.515 (0.0004)	254 (11)	24 (8)	1.98
G28.83–0.25_W	18:44:50.744 (0.001)	-3:45:49.33 (0.04)	142 (10)	21 (11)	2.17

[a] The association of these 1.3 cm detections with the EGO is unclear, and neither 1.3 cm source has a 1.3 mm counterpart. The listed 1.3 mm flux densities are upper limits, obtained by measuring the 1.3 mm flux density with a beam-sized aperture at the location of the 1.3 cm source and at a reasonable, nearby off-position. The spectral indices listed assume that the 1.3 mm flux upper limit is a precise value.

Conclusions and Future Work

Our analysis of the spectral indices of our new 1.3 cm detections shows that none of these objects has a steep enough spectral index for its 1.3 cm emission to be attributable to dust emission alone. The spectral indices indicate that there is likely free-free or synchrotron emission present in all cases, and the low 1.3 cm flux densities show that this emission is weak. This is consistent with the notion that this is a class of protostellar objects in which centimeter-wavelength continuum emission is just beginning to emerge.

We currently have or are in the process of obtaining additional observations of these sources at 5 cm (JVLA C-band) and 3.2 mm (ALMA Band 3). With these additional data, we expect to be able to constrain the radio-wavelength spectral energy distributions (SEDs) of these sources. Constraining the SEDs will allow us to address two key areas of massive protocluster research: 1) Well-sampled SEDs for the individual protostars enable us to disentangle the various types of centimeter-wavelength continuum emission (dust, free-free, synchrotron, etc.) for each protostar through analysis of their spectral indices. The high angular resolution enables us to further refine the specific emission mechanisms (e.g. gravitationally-trapped HC HII region, ionized jet, stellar wind, etc.) by examining emission morphology. 2) Determining these emission mechanisms will help us to determine the demographics (evolutionary stage, mass, clustering, mass segregation if any) of the population within each protocluster, which is a key prediction of current competing theories of massive star-formation.

References:

Cyganowski, C. J., et al 2008, AJ, 136, 2391
Cyganowski, C. J., et al. 2009, ApJ, 702, 1615
Cyganowski, C. J., et al. 2013, ApJ, 764, 61
Green, J. A., et al. 2010, MNRAS, 409, 913